International Journal of Solids and Structures 124 (2017) 252–263

Contents lists available at ScienceDirect

International Journal of Solids and Structures

journal homepage: www.elsevier.com/locate/ijsolstr

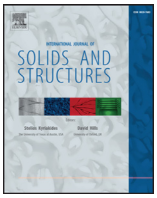

# A constitutive model of shape memory polymers based on glass transition and the concept of frozen strain release rate

Yunxin Li, Jianying Hu, Zishun Liu*

*International Center for Applied Mechanics, State Key Laboratory for Strength and Vibration of Mechanical Structures, Xi'an Jiaotong University, Xi'an 710049, People's Republic of China*

ARTICLE INFO

*Article history:*
Received 16 March 2017
Revised 17 June 2017
Available online 30 June 2017

*Keyword:*
Shape memory effect
Shape memory polymer
Thermomechanical behaviors
Constitutive model
Time factor

ABSTRACT

Shape memory polymers (SMPs) are a type of polymeric smart material. They can maintain a deformed shape and return to their original shape according to external stimuli, such as temperature, light, pH, magnetic field and so on. In the last decade, SMPs have gained increasing attention due to their unique properties and have thus led great progress in developing proper constitutive models. In this paper, we propose and establish a new phase-evolution-based thermomechanical constitutive model for amorphous SMPs by considering the materials as a mixture of the rubbery phase and glassy phase. The shape memory effect (SME) is captured under the assumption that the rubbery phase can transform into the glassy phase and that part of the strain will be frozen during the glass transition. To make the model be more feasible, furthermore, we improve the model by introducing a time factor and considering the influence of frozen strain release rate. To validate the robustness and applicability of the proposed new model, we reproduce the shape memory behaviors (SMBs) of two different materials under different constraints and conditions. The results show a remarkable consistency between the new model simulation and experimental data.

## 1. Introduction

Shape memory polymers (SMPs) are a type of polymeric smart material that can maintain a deformed state (temporal shape) and return to their original state (permanent shape) under different external stimulus conditions. For example, they can be deformed under pre-deformation at a high temperature and maintain the deformed state when cooled to a lower temperature. When the temperature is increased again, their permanent shape can be recovered. Compared to other smart materials, *e.g.*, shape memory alloys (SMAs) (Ashrafi et al., 2016; Oliveira et al., 2014; Poorasadion et al., 2015) and shape memory ceramics (SMCs) (Matsumura et al., 2011), SMPs have many advantages, such as a large restorable strain, large elastic deformation, biodegradability, biocompatibility, light weight, low cost, and excellent manufacturability (Baghani et al., 2012; Diani et al., 2012; Leng et al., 2009). Due to their unique properties, SMPs have a promising future with many potential applications, including as morphing structures, biomedical devices, functional textiles, active aircraft equipment, aerospace structures, self-healing materials, 3D printing and pattern transformation devices (Behl et al., 2010; Ge et al., 2014; Ge et al., 2016; Ghosh et al., 2013; He et al., 2015; Hu et al., 2012; Hu and Chen, 2010; Huang et al., 2013; Liu et al., 2015; Rossiter et al., 2014; Xie, 2010; Xu et al., 2010).

To capture the complex thermomechanical mechanisms and describe the shape memory behavior (SMB) of SMPs, many constitutive models had been proposed in the past two decades. Tobushi et al. (1997) developed a linear viscoelastic constitutive model to describe the temperature- and time-dependent shape memory effect (SME) of polyurethane. This model combined the Maxwell model with a friction element and is able to qualitatively evaluate the thermomechanical properties of polyurethane. Tobushi et al. (2001) further modified their previous linear model into a nonlinear one in which the parameters of materials were expressed by single expansion functions of temperature and described the relationship between the modulus and temperature. Based on viscoelastic theory, Lin and Chen (1999) established another thermoviscoelastic model to provide a description of the rate-dependent behavior of polyurethanes. They confirmed that a good prediction of the SMB of polyurethanes could be obtained by their model. Morshedian et al. (2005) developed a thermo-viscoelastic constitutive theory to characterize the shape fixability and shape recoverability of polyethylene. This is a unique thermomechanical constitutive theory for Tm-type SMPs that uses the crystal melting

---

* Corresponding author.
*E-mail addresses:* zishunliu@mail.xjtu.edu.cn, zishunliu@nus.edu.sg (Z. Liu).

http://dx.doi.org/10.1016/j.ijsolstr.2017.06.039
0020-7683/

temperature as a switch control unit to capture their shape memory capability (Hu et al., 2012). To provide a simpler and more effective prediction method for SMPs, a succinct three-element model was presented by Li et al. (2015). Although it is simple, their model evaluates the thermomechanical properties of SMPs and is particularly convenient and concise when the temperature-dependent Young's modulus, viscosity coefficient, and relaxation time of SMPs are determined through experiments. All of the above viscoelastic constitutive models use rheological models composed of the dashpot element, spring element and frictional element. These discrete models could not only qualitatively describe the behavior of SMPs, but they could also capture the temperature and time dependence of shape recovery. They have played an important role in SMPs research. However, beyond the thermo-viscoelastic model, one other approach, phase transition approach, is also widely used.

Based on considerable experimental data and a deep understanding of the molecule mechanisms of SME, Liu et al. (2006) developed one of the first phenomenological continuum constitutive models for SMPs (Baghani et al., 2012). Their continuum model viewed SMPs as a continuum mixture of two different phases: the frozen phase (hard phase) and active phase (soft phase), which have a clear physical meaning. In their model, two internal state variables (*i.e.*, the frozen phase volume fraction and stored strain) are used to describe the evolution of the structural transformation of SMPs. Their model is in agreement with the micromechanism of glass transition and can predict the SMB of an epoxy well; however, their model is also limited to a specific type of shape memory material. Additionally, the time-dependency of the material behaviors are not considered in their simplified model. Moreover, the mathematical evolution law is only applicable to the cooling process; a mathematical formulation for the heating process is not present (Baghani et al., 2012; Chen and Lagoudas, 2008a,b; Yang and Li, 2016).

Based on the evolution of deformation energy switching from an entropy dominated state to an enthalpy dominated state, a constitutive model of semicrystalline SMPs was proposed by Qi et al. (2008). They further developed similar constitutive equations to describe both 1-Way and 2-Way SME effects, which were demonstrated previously (Westbrook et al., 2010). In their models, the SME was captured by assuming that the newly formed crystals were formed in a stress-free (natural) configuration during the crystallization process (Ge et al., 2012; Rajagopal and Srinivasa, 1998a, b). This meant that the newly formed phase was undeformed immediately upon its formation. A similar assumption for amorphous SMPs can be put forward during the glass transition: the rubbery phase transforms into a glassy phase and part of the strain is frozen. Using this reasonable assumption, the SME of amorphous SMPs can be effectively captured.

In this work, a new continuum thermomechanical constitutive model based on the concept of glass transition is developed to describe the SMBs of amorphous SMPs. We use a similar assumption as in Liu's model (Liu et al., 2006), that the material is a mixture of a rubbery phase and a glassy phase, which is in agreement with the micromechanism of the glass transition. This successfully relates the glass transition to SME. To make the model be more feasible, furthermore, we improve this continuum model by introducing a time factor. To show the validity and applicability of our model, we reproduce the SMBs of two different materials. Good agreement is observed between the model simulation and experimental results.

The remainder of the paper is organized as follows. In Section 2, a new continuum thermomechanical constitutive model for shape memory polymers is proposed and developed; the model is then utilized to consider the SME of materials. The temperature variable functions and material parameters are determined in Section 3. In Section 4, the results predicted by our present model are compared to the experimental results. Finally, we draw concluding remarks in Section 5.

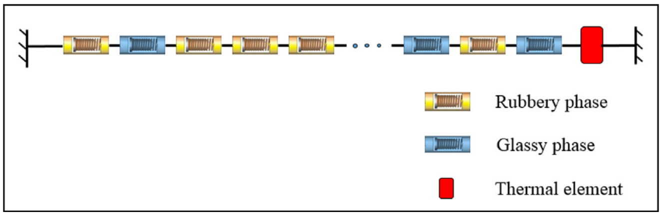

**Fig. 1.** Schematic representation of the proposed constitutive model.

## 2. Constitutive model

### 2.1. Overall model description

In this section, a new phase-evolution-based thermomechanical constitutive model for amorphous SMPs is developed. We assume that the shape memory material is a mixture of a rubbery phase and glassy phase as previously performed in similar works (*e.g.*, Baghani et al., (2012); Li et al., (2017); Liu et al., (2006)). Because the phase transition of materials is a continuous process, we further divide the rubbery phase into many small rubbery phase domains with the volume fraction $\Delta\gamma_r^j$ and divide the glassy phase into many small glassy phase domains with the volume fraction $\Delta\gamma_g^j$. The volume fractions satisfy $\Sigma\Delta\gamma_g^j + \Sigma\Delta\gamma_r^j = 1$. Fig. 1 shows the 1D schematic of the phase-evolution-based thermomechanical model. Two types of springs in the schematic, the rubbery phase (in yellow) and glassy phase (in pewter), can be transformed into each other, reflecting the process of phase transition. When the temperature decreases, some of the rubbery phase domains are transformed into the newly formed glassy phase domains, which is consistent with the glass transition process (Matsuoka, 1992; Strobl, 1997). The ratio of these two types of springs corresponds to the volume fraction of the respective phase, which varies with the instantaneous temperature. The variation of this ratio with temperature embodies the glass transition, and the SME can be acquired during the thermomechanical cycle.

In addition, a thermal deformation element is used to represent thermal expansion and contraction. Following some previous works ((Baghani et al., 2012; Chen and Lagoudas, 2008a; Ju et al., 2010; Liu et al., 2006), the deformation gradient in SMP is decomposed into rubbery, glassy, and thermal components. Thus, the total deformation gradient of model $\boldsymbol{F}$ can be decomposed as: $\boldsymbol{F}=\boldsymbol{F}_r\boldsymbol{F}_g\boldsymbol{F}_T$, where $\boldsymbol{F}_r$, $\boldsymbol{F}_g$ and $\boldsymbol{F}_T$ represent the deformation gradients of the rubbery phase, glassy phase and thermal deformation, respectively. For our 1D thermomechanical model, which is limited to a small strain and linear elastic behavior, the deformations are considered to be in a uniaxial tensile state and the deformation gradients can be replaced by linear strains. The total strain is given by:

$$\varepsilon_{total} = \Sigma\Delta\gamma_r^j\varepsilon^j_{rubbery} + \Sigma\Delta\gamma_g^j\varepsilon^j_{glassy} + \varepsilon_T \tag{1}$$

where $\varepsilon_T$ is the thermal strain, $\varepsilon^j_{rubbery}$ is the strain in the *j*th rubbery phase domain with a volume fraction of $\Delta\gamma_r^j$ and $\varepsilon^j_{glassy}$ is the strain the *j*th glassy phase domain with a volume fraction of $\Delta\gamma_g^j$.

Because the model consists of elements in a series (Fig. 1), the stresses in all of the domains are equal in this model. The total stress is:

$$\sigma_{total} = \sigma_r = \sigma_g \tag{2}$$

where $\sigma_r$ is the stress in the rubbery phase domains and $\sigma_g$ is the stress in the glassy phase domains.

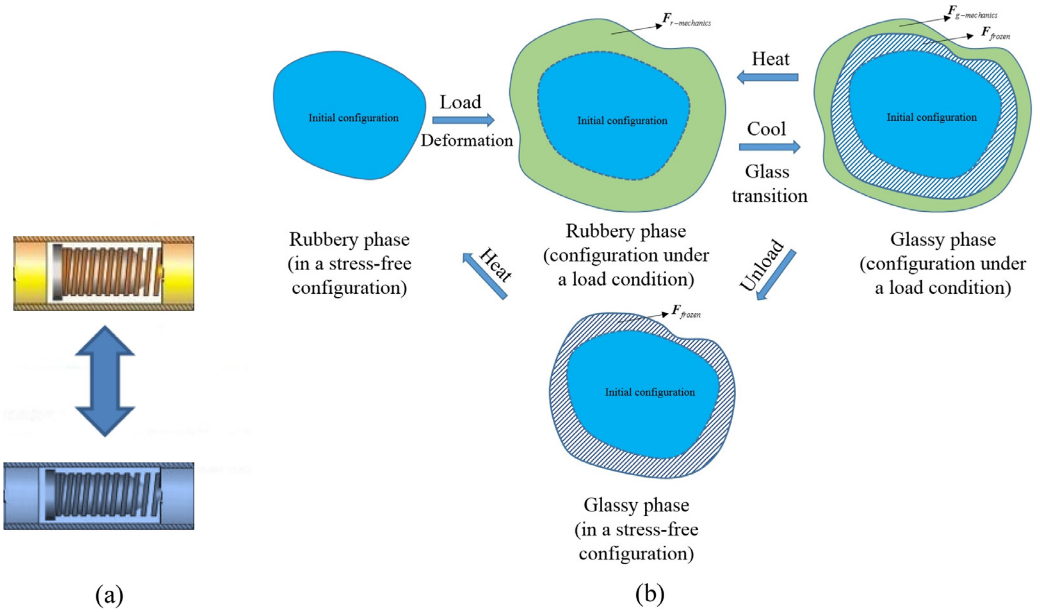

**Fig. 2.** Schematic illustration of the SME mechanism: (a) schematic representation of a phase transition from the rubbery phase to the glassy phase, and vice versa; (b) schematic representation of typical thermomechanical cycles of SMPs.

These two types of springs in the rubbery phase domains and glassy phase domains can be transformed into each other (as shown in Fig. 2(a)). This transformation represents a glass transition, and the SME can be captured by the model during the thermomechanical cycle. The SME process, accompanied by a phase transition, is further described in Fig. 2(b). To emphasize the mechanical aspect of the model, we ignore the thermal strain during the phase transition. Thermal contraction/expansion is included when considering the SME. As illustrated in Fig. 2(b), a rubbery phase domain undergoes a mechanical deformation $\boldsymbol{F}_{r-mechanics}$ under an external force. With the temperature reduction, when the rubbery phase domain experiences a phase transition and transforms into a glassy phase domain, part of the deformation in the glassy phase will be frozen. The frozen deformation is denoted by $\boldsymbol{F}_{frozen}$. The residual mechanical deformation in the glassy phase domain is denoted by $\boldsymbol{F}_{g-mechanics}$. If the glassy phase domain is heated under strain constraints, the glassy phase domain transforms back into the rubbery phase domain and the frozen deformation will be released. If the glassy phase domain is unloaded, the residual mechanical deformation $\boldsymbol{F}_{g-mechanics}$ will disappear and only the frozen deformation $\boldsymbol{F}_{frozen}$ will be retained. According to the above analysis, for our 1D thermomechanical model, we can see that there is only a mechanical strain $\varepsilon_{r-mechanics}$ in the rubbery phase domains. While in the glassy phase domains, the strain includes the mechanical strain $\varepsilon_{g-mechanics}$ and frozen strain $\varepsilon_{frozen}$. Thus, the strain in the $j$th rubbery phase domain satisfies $\varepsilon_{rubbery}^{j} = \varepsilon_{r-mechanics}^{j}$, and the strain in the $j$th glassy phase domain obeys $\varepsilon_{glassy}^{j} = \varepsilon_{g-mechanics}^{j} + \varepsilon_{frozen}^{j}$.

Then, the total strain of the model can be written as:

$$\varepsilon_{total} = \Sigma\Delta\gamma_r^j\varepsilon_{r-mechanics}^j + \Sigma\Delta\gamma_g^j\left(\varepsilon_{g-mechanics}^j + \varepsilon_{frozen}^j\right) + \varepsilon_T \quad (3)$$

For these two types of spring elements in the model, the constitutive relationships are generally described by Hooke's law.

$$\sigma_r = E_r\varepsilon_{r-mechanics}^j, \quad \mathrm{j} = 1, 2, 3\ldots \quad (4)$$

$$\sigma_g = E_g\varepsilon_{g-mechanics}^j, \quad \mathrm{j} = 1, 2, 3\ldots \quad (5)$$

where $E_r$ and $E_g$ are the Young's modulus of the rubbery phase domains and glassy phase domains, respectively. From Eq. (2), we know that the stresses in all of the domains are equal. Therefore, the strains in all of the rubbery phase domains are equal, which can be denoted by $\varepsilon_{r-mechanics}$. Thus, for any $j$, the mechanical strain in the $j$th rubbery phase domain is: $\varepsilon_{r-mechanics}^j = \varepsilon_{r-mechanics}$. Similarly, for any $j$, the mechanical strain in the $j$th glassy phase domain is: $\varepsilon_{g-mechanics}^j = \varepsilon_{g-mechanics}$. Then, the total strain in Eq. (3) can be simplified as:

$$\varepsilon_{total} = \Sigma\Delta\gamma_r^j\varepsilon_{r-mechanics} + \Sigma\Delta\gamma_g^j\left(\varepsilon_{g-mechanics} + \varepsilon_{frozen}^j\right) + \varepsilon_T \quad (6)$$

We define an internal variable fraction of glassy phase $\gamma$ to be:

$$\gamma = \Sigma\Delta\gamma_g^j \quad (7)$$

Then, the fraction of the rubbery phase can be obtained:

$$\Sigma\Delta\gamma_r^j = 1 - \gamma \quad (8)$$

Inserting Eqs. (7) and (8) into Eq. (6), the total strain can be rewritten as:

$$\varepsilon_{total} = (1-\gamma)\varepsilon_{r-mechanics} + \gamma\varepsilon_{g-mechanics} + \Sigma\Delta\gamma_g^j\varepsilon_{frozen}^j + \varepsilon_T \quad (9)$$

The total strain can be further generalized as:

$$\varepsilon_{total} = \varepsilon_m + \varepsilon_f + \varepsilon_T \quad (10)$$

where $\varepsilon_m = (1-\gamma)\varepsilon_{r-mechanics} + \gamma\varepsilon_{g-mechanics}$ represents the total mechanical strain in the materials and $\varepsilon_f = \Sigma\Delta\gamma_g^j\varepsilon_{frozen}^j$ represents the total frozen strain in the materials.

### *2.2. Shape memory effect*

In this section, we describe the SME with our continuum thermomechanical constitutive model.

To develop a comparatively simple modeling approach to explain the complex thermomechanical phenomena, some level-of-detail comprehensions are sacrificed, and therefore, several assumptions are made:

(1) During the glass transition, the rubbery phase domains transform into glassy phase domains and part of the strain will be frozen (as shown in Fig. 2(b)). For the simplicity of the model, it is assumed that the residual mechanical strain $\varepsilon_{g-mechanics}^{*}$

in the newly formed glassy phase domains is a linear function of the initial mechanical strain $\varepsilon_{r-mechanics}$ from the previous rubbery phase domains:

$$\varepsilon_{g-mechanics}{}^{*} = f(T)\varepsilon_{r-mechanics} \tag{11}$$

where *f*(*T*) is a function of temperature. The detailed explanation of this assumption is given by using the free-volume theory (Fox and Loshaek, 1955) in the following sub-section.

(2) Previous studies (Barot and Rao, 2006; Qi et al., 2008) assumed that no significant deformation of the material occurs during the formation of the new phase. Therefore, we assume that during every glass transition process, the total strain of the material $\varepsilon^{total}$ remains constant.

(3) For a better understanding of the thermodynamics of SMPs, we adopt an incremental approach to describe the thermomechanical cycle. Once the temperature decreases by $\Delta T$, there will be a small volume fraction of the rubbery phase domain that transforms into the glassy phase domain, in which the modulus and mechanical strain are changed. While the other domains that are not involved in the glass transition remain the same, to meet the boundary conditions, the stress-strain field in the material should be re-distributed. This process is instantaneous (Ge et al., 2012; Westbrook et al., 2010); thus, we assume that during the redistribution of stress, the total strain $\varepsilon^{total}$ and total mechanical strain $\varepsilon_m$ remain the same.

(4) To simplify the model, the glass transition process is divided into three steps with the temperature change $\Delta T$. A similar assumption has been used by others to consider the SME (Ge et al., 2012, 2013; Westbrook et al., 2010). In step 1, there is only thermal expansion/contraction but no phase transition in the material. In step 2, a small volume fraction of a domain undergoes a glass transition, while the other domains, which are not involved in the glass transition, remain the same. In this state, the force is no in equilibrium, and the stress-strain field in the material will be re-distributed in the next step. Therefore, step 3 is the redistribution of stress.

### 2.2.1. Mechanics behavior during the cooling process

Assuming that the thermomechanical loading process starts at a high temperature $T=T_h$, the material consists of a 100% rubbery phase and the variable fraction of glassy phase is $\gamma=0$. Therefore,

$$\varepsilon^0_{total} = \varepsilon^0_m + \varepsilon^0_f + \varepsilon^0_T \tag{12}$$

where $\varepsilon^0_{total}$, $\varepsilon^0_m$, $\varepsilon^0_f$ and $\varepsilon^0_T$ are the strains in the initial rubbery phase (denoted by superscript 0).

At $T=T_h$, $\gamma=0$,

$$\varepsilon^0_f = 0,\ \varepsilon^0_m = \varepsilon^0_{r-mechanics}, \tag{13}$$

The glass transition starts at temperature $T=T_h$ in the cooling process. When the temperature changes from $T=T_h$ to $T=T_h+\Delta T$, where $\Delta T < 0$, a small amount of the rubbery phase transformed into the glassy phase with a volume fraction $\Delta\gamma_1$. As stated above, we divide the glass transition process into three steps.

At step 1, there is no phase transition, only thermal contraction. Then, the total strain is:

$$\varepsilon^1_{total} = \varepsilon^0_m + \varepsilon^0_f + \varepsilon^1_T \tag{14}$$

At step 2, the rubbery phase domain that has a volume fraction $\Delta\gamma_1$ experiences a phase transition and transforms into a glassy phase domain. Thus, part of the strain will be frozen and the mechanical strain is changed. The new frozen strain and total mechanical strain at the first temperature increment are denoted by $\varepsilon^1_f$ and $\varepsilon^1_{m,}$ respectively. The total strain at temperature $T=T_h+\Delta T$ becomes:

$$\varepsilon^1_{total} = \varepsilon^1_m + \varepsilon^1_f + \varepsilon^1_T \tag{15}$$

During this glass transition, the mechanical strain in the small volume fraction domain $\Delta\gamma_1$ is changed while the other domains, which are not involved in the glass transition, retain the same mechanical strain. According to Eq. (10), we can obtain the total mechanical strain:

$$\varepsilon^1_m = \Delta\gamma_1\varepsilon^0_{g-mechanics} * + (1-\Delta\gamma_1)\varepsilon^0_{r-mechanics} \tag{16}$$

where $\varepsilon^0_{g-mechanics}*$ is the residual mechanical strain in the newly formed glassy phase domain. We assume that the mechanical strain of this newly formed glassy phase is:

$$\varepsilon^0_{g-mechanics}{}^{*} = f(T)\varepsilon^0_{r-mechanics} \tag{17}$$

At step 3, to achieve stress equilibrium, the stress-strain field in the material will be re-distributed.

In the state of stress equilibrium, the mechanical strains in all of the rubbery phase domains are equal (denoted by $\varepsilon^1_{r-mechanics}$) and the mechanical strains in all of the glassy phase domains are equal (denoted by $\varepsilon^1_{g-mechanics}$). Similar to Eq. (16), the total mechanical strain after step 3 becomes:

$$\varepsilon^1_m = \Delta\gamma_1\varepsilon^1_{g-mechanics} + (1-\Delta\gamma_1)\varepsilon^1_{r-mechanics} \tag{18}$$

and the total stress is:

$$\sigma^1_{total} = \sigma_r{}^1 = \sigma^1_g \tag{19}$$

where $\sigma^1_r = E_r\varepsilon^1_{r-mechanics}$ and $\sigma^1_g = E_g\varepsilon^1_{g-mechanics}$.

Inserting Eqs. (15) and (18) into Eq. (19), we have:

$$\sigma^1_{total} = \frac{\varepsilon^1_{total} - \varepsilon^1_f - \varepsilon^1_T}{\frac{\Delta\gamma_1}{E_g} + \frac{1-\Delta\gamma_1}{E_r}} \tag{20}$$

Comparing Eq. (14) and Eq. (15), we obtain:

$$\varepsilon^1_f - \varepsilon^0_f = \varepsilon^0_m - \varepsilon^1_m \tag{21}$$

Incorporating Eqs. (13) and (16) into Eq. (21), the small incremental frozen strain $\Delta\varepsilon^1_f$ at the first temperature increment becomes:

$$\begin{aligned}\Delta\varepsilon^1_f &= \varepsilon^1_f - \varepsilon^0_f = \Delta\gamma_1[1-f(T)]\varepsilon^0_m \\ &= \Delta\gamma_1[1-f(T)]\left(\varepsilon^0_{total} - \varepsilon^0_f - \varepsilon^0_T\right)\end{aligned} \tag{22}$$

In the process of temperature change from $T=T_h+(i-1)\Delta T$ to $T=T_h+i\Delta T$, where $\Delta T < 0$, a small amount of the rubbery phase transformed into the glassy phase with a volume fraction $\Delta\gamma_i$. The glass transition process is also divided into 3 steps.

In step 1, the *i*th phase transition has not yet occurred. The total strain is:

$$\varepsilon^i_{total} = \varepsilon^{i-1}_m + \varepsilon^{i-1}_f + \varepsilon^i_T \tag{23}$$

where the total mechanical strain in the (*i-1)*th phase transition is:

$$\varepsilon^{i-1}_m = \sum_{j=1}^{i-1}\Delta\gamma_j\varepsilon^{i-1}_{g-mechanics} + \left(1-\sum_{j=1}^{i-1}\Delta\gamma_j\right)\varepsilon^{i-1}_{r-mechanics} \tag{24}$$

In step 2, the *i*th phase transition occurs in the rubbery phase domain with a volume fraction $\Delta\gamma_i$. The total strain at temperature $T=T_h+i\Delta T$ becomes:

$$\varepsilon^i_{total} = \varepsilon^i_m + \varepsilon^i_f + \varepsilon^i_T \tag{25}$$

During the *i*th phase transition, the mechanical strain in the small volume fraction domain $\Delta\gamma_i$ changes, while the other domains, which are not involved in this glass transition, remain under the same mechanical strain. Thus, the total mechanical strain is:

$$\varepsilon_m^i = \sum_{j=1}^{i-1} \Delta\gamma_j \varepsilon_{g-mechanics}^{i-1} + \Delta\gamma_i \varepsilon_{g-mechanics}^{i-1}{}^* + \left(1 - \sum_{j=1}^{i} \Delta\gamma_j\right) \varepsilon_{r-mechanics}^{i-1} \tag{26}$$

We assume that the residual mechanical strain$\varepsilon_{g-mechanics}^{i-1}{}^*$in the $i$th newly formed glassy phase domain $\Delta\gamma_i$ is:

$$\varepsilon_{g-mechanics}^{i-1}{}^* = f(T)\varepsilon_{r-mechanics}^{i-1} \tag{27}$$

In step 3, the stress-strain field in the material will be redistributed. Similarly, with Eqs. (18) and (19), the total mechanical strain after step 3 becomes:

$$\varepsilon_m^i = \sum_{j=1}^{i} \Delta\gamma_j \varepsilon_{g-mechanics}^{i} + \left(1 - \sum_{j=1}^{i} \Delta\gamma_j\right) \varepsilon_{r-mechanics}^{i} \tag{28}$$

and the total stress is:

$$\sigma_{total}^i = \sigma_r^i = \sigma_g^i \tag{29}$$

where $\sigma_r^i = E_r \varepsilon_{r-mechanics}^i$ and $\sigma_g^i = E_g \varepsilon_{g-mechanics}^i$.

Inserting Eqs. (25) and (28) into Eq. (29), we have:

$$\sigma_{total}^i = \frac{\varepsilon_{total}^i - \varepsilon_f^i - \varepsilon_T^i}{\frac{\sum_{j=1}^{i} \Delta\gamma_j}{E_g} + \frac{1-\sum_{j=1}^{i} \Delta\gamma_j}{E_r}} \tag{30}$$

Comparing Eq. (23) and Eq. (25), we obtain:

$$\varepsilon_f^i - \varepsilon_f^{i-1} = \varepsilon_m^{i-1} - \varepsilon_m^i \tag{31}$$

Incorporating Eqs. (24) and (26) into Eq. (31), the small incremental frozen strain$\Delta\varepsilon_f^i$ at the $i$th temperature increment becomes:

$$\begin{aligned}\Delta\varepsilon_f^i &= \varepsilon_f^i - \varepsilon_f^{i-1} = \Delta\gamma_i[1 - f(T)]\varepsilon_{r-mechanics}^{i-1} \\ &= \Delta\gamma_i[1 - f(T)]\frac{\varepsilon_{total}^{i-1} - \varepsilon_f^{i-1} - \varepsilon_T^{i-1}}{E_r\left(\frac{\sum_{j=1}^{i-1} \Delta\gamma_j}{E_g} + \frac{1-\sum_{j=1}^{i-1} \Delta\gamma_j}{E_r}\right)}\end{aligned} \tag{32}$$

Note that $\varepsilon_{total}^i$, $\varepsilon_m^i$, $\varepsilon_f^i$ and $\varepsilon_T^i$ in Eqs. (23)–(32) are the strains at the $i$th temperature increment (denoted by superscript $i$).

At temperature $T = T_h + i\Delta T$, the fraction of glassy phase $\gamma_i$ is $\gamma_i = \sum_{j=1}^{i} \Delta\gamma_j$, and Eqs. (30) and (32) can be simplified as follows:

$$\sigma_{total}^i = \frac{\varepsilon_{total}^i - \varepsilon_f^i - \varepsilon_T^i}{\frac{\gamma_i}{E_g} + \frac{1-\gamma_i}{E_r}} \tag{33}$$

$$\Delta\varepsilon_f^i = \Delta\gamma_i[1 - f(T)]\frac{\varepsilon_{total}^{i-1} - \varepsilon_f^{i-1} - \varepsilon_T^{i-1}}{E_r\left(\frac{\gamma_{i-1}}{E_g} + \frac{1-\gamma_{i-1}}{E_r}\right)} \tag{34}$$

When both the left and right sides of Eq. (34) are divided by the temperature increment $\Delta T$, Eq. (34) becomes:

$$\frac{\Delta\varepsilon_f^i}{\Delta T} = \frac{\Delta\gamma_i}{\Delta T}[1 - f(T)]\frac{\varepsilon_{total}^{i-1} - \varepsilon_f^{i-1} - \varepsilon_T^{i-1}}{E_r\left(\frac{\gamma_{i-1}}{E_g} + \frac{1-\gamma_{i-1}}{E_r}\right)} \tag{35}$$

As the temperature increment $\Delta T$ becomes infinitely small, the limit value of the ratio of the differences $\Delta\varepsilon_f^i/\Delta T$ and $\Delta\gamma_i/\Delta T$ can be written as the derivative of $\varepsilon_f$ with respect to $T$, $d\varepsilon_f/dT$, and the derivative of $\gamma$ with respect to $T$, $d\gamma/dT$, respectively. Thus, a differential formation of Eq. (35) is:

$$\frac{d\varepsilon_f}{dT} = \frac{d\gamma}{dT}[1 - f(T)]\frac{\varepsilon_{total} - \varepsilon_f - \varepsilon_T}{E_r\left(\frac{\gamma}{E_g} + \frac{1-\gamma}{E_r}\right)} \tag{36}$$

Thus, the mechanics behavior of SMPs during cooling can be described by the following constitutive equations:

$$\begin{cases} \sigma_{total} = \frac{\varepsilon_{total} - \varepsilon_f - \varepsilon_T}{\frac{\gamma}{E_g} + \frac{1-\gamma}{E_r}} \\ \frac{d\varepsilon_f}{dT} = \frac{d\gamma}{dT}[1 - f(T)]\frac{\varepsilon_{total} - \varepsilon_f - \varepsilon_T}{E_r\left(\frac{\gamma}{E_g} + \frac{1-\gamma}{E_r}\right)} \end{cases} \tag{37}$$

The evolution of the frozen strain $\varepsilon_f$ and constitutive equations in Eq. (37) are consistent with the thermodynamic microscopic interpretation that the micro-Brownian motion is affected by temperature (Tobushi et al., 2001). During the cooling process, the micro-Brownian motion of molecular chains recedes. The macroscopic manifestation is that a portion of the strain is frozen and the deformed shape is maintained. As the temperature increases, the frozen strain decreases and the original shape is gradually recovered due to the micro-Brownian motion of molecular chains activated by heating (Tobushi et al., 2001).

### *2.2.2. Mechanics behavior during the heating process*

At the low temperature $T = T_l$, the material consists of 100% glassy phase; thus, the initial fraction of the glassy phase $\gamma$ is 1. During heating, the glassy phase domains gradually disappear. As the temperature changes from $T = T_l + (i-1)\Delta T$ to $T = T_l + i\Delta T$, where $\Delta T > 0$, a small amount of the glassy phase transforms into the rubbery phase with a volume fraction $-\Delta\gamma_i$. The fraction of the glassy phase becomes $(1 + \sum_{j=1}^{i} \Delta\gamma_j)$, and the fraction of the rubbery phase is $(0 - \sum_{j=1}^{i} \Delta\gamma_j)$.

During heating, the glass transition process is also divided into three steps. At step 1, the $i$th phase transition has not occurred yet. There is only thermal expansion. Then, at step 2, the $i$th phase transition occurs. According to Eq. (27), if the temperature increases by$\Delta T$ at temperature $T = T_l + i\Delta T$, the frozen strain at this temperature increment is $(1 - f(T))\varepsilon_{r-mechanics}^{i-1}$. Thus, we assume that during heating, the $i$th newly formed rubbery phase domain will release $(1 - f(T))\varepsilon_{r-mechanics}^{i-1}$ on the basis of the initial mechanical strain in the glassy state. Then, we can obtain the mechanical strain in the $i$th newly formed rubbery phase domain. In step 3, after the stress reaches equilibrium, the total strain and total stress can be obtained.

Similarly, in Eq. (37), the constitutive equations of SMPs during heating can be solved as:

$$\begin{cases} \sigma_{total} = \frac{\varepsilon_{total} - \varepsilon_f - \varepsilon_T}{\frac{\gamma}{E_g} + \frac{1-\gamma}{E_r}} \\ \frac{d\varepsilon_f}{dT} = \frac{d\gamma}{dT}[1 - f(T)]\frac{\varepsilon_{total} - \varepsilon_f - \varepsilon_T}{E_r\left(\frac{\gamma}{E_g} + \frac{1-\gamma}{E_r}\right)} \end{cases} \tag{38}$$

This is the same as the process during cooling, which is in agreement with the experimental investigations. Under the same boundary condition, the stress evolution paths during heating almost exactly overlay the stress–temperature curves during cooling (Liu et al., 2006).

## *2.3. Thermal deformation*

The thermal expansion and contraction effects, which are assumed to be independent of the mechanical properties (Li et al., 2015; Tobushi et al., 1997, 2001), are represented as thermal strain $\varepsilon_T$:

$$\varepsilon_T = \int_{T_0}^{T} \alpha dT \tag{39}$$

where $\alpha$ is the coefficient of thermal expansion (CTE) and $T_0$ is the reference temperature.

### 2.4. Further improvement of the model

We have developed a phase-evolution-based constitutive model in Sections 2.1–2.3. Similar to some important SMPs works (*e.g.*, Liu et al., (2006), Chen and Lagoudas (2008a, b)), in the model proposed before, the frozen strain is a function of temperature and assumed to be independent of time, but that is an idealized case. In an actual situation, it takes a certain amount of time to freeze the strain. This model simplification may compromise the reliability of the method. To make the model be more feasible, we further improve the model by introducing a time factor in this sub-section.

#### 2.4.1. Frozen strain release rate

First, we propose the concept of a frozen strain release rate. Unlike the frozen strain in our original model, in an actual situation, with the change of temperature, the strain of the freezing process takes a certain amount of time to complete. When the temperature changes $\Delta T$, if the time $\Delta t$ is long enough, the freezing can be fully completed and the change of the frozen strain in reality ($\Delta\varepsilon_{f-real}$) can achieve the theoretical value $\Delta\varepsilon_f$ from our original model. If the time $\Delta t$ is very short, freezing cannot fully occur and the change of the frozen strain in reality ($\Delta\varepsilon_{f-real}$) will be smaller than the theoretical value. Thus, we introduce a function of time: the frozen strain release rate $G(t)$. This rate is defined as the ratio of $\Delta\varepsilon_{f-real}$ to $\Delta\varepsilon_f$ and changes from 0 to 1 over time. When time $t=0$, freezing has not yet occurred. As such, $G(0)=0$. At time $t=\infty$, freezing has fully occurred. As such, $G(\infty)=1$. Considering the two limiting cases, $G(0)=0$ and $G(\infty)=1$, the frozen strain release rate $G(t)$ is defined as:

$$G(t) = 1 - e^{-\frac{t}{\tau}} \tag{40}$$

where $\tau$ is the material parameter that is calibrated through trial and error to fit the experimental data.

According to the definition of $G(t)$, we have:

$$\Delta\varepsilon_{f-real} = \Delta\varepsilon_f G(t) = \Delta\varepsilon_f\left(1 - e^{\frac{-\Delta t}{\tau}}\right) \tag{41}$$

#### 2.4.2. Evolution of the frozen strain in reality $\varepsilon_{f-real}$

Here, we assume that at time $t=0$ and temperature $T=T_0$, the initial frozen strain is$\varepsilon_f^0$.

At time $t=\Delta t$ and temperature $T=T_0+\Delta T$, the change of the frozen strain in the original model is $\Delta\varepsilon_f^1$ at the first temperature increment. The change of the frozen strain in reality $\Delta\varepsilon_{f-real}^{11}$ and actual strain $\varepsilon_{f-real}^1$ become:

$$\Delta\varepsilon_{f-real}^{11} = \Delta\varepsilon_f^1\left(1 - e^{\frac{-\Delta t}{\tau}}\right) \text{and}\, \varepsilon_{f-real}^1 = \varepsilon_f^0 + \Delta\varepsilon_f{}^1 - \left(\Delta\varepsilon_f^1 e^{\frac{-\Delta t}{\tau}}\right) \tag{42}$$

where $\Delta\varepsilon_{f-real}^{11}$ is the actual release value of $\Delta\varepsilon_f^1$ at time $t=\Delta t$.

At time $t=2\Delta t$ and temperature $T=T_0+2\Delta T$, the change of the frozen strain in the original model is $\Delta\varepsilon_f^2$ at the second temperature increment. The changes of the frozen strains in reality are:

$$\Delta\varepsilon_{f-real}^{22} = \Delta\varepsilon_f^2\left(1 - e^{\frac{-\Delta t}{\tau}}\right) \text{and}\, \Delta\varepsilon_{f-real}^{12} = \Delta\varepsilon_f^1\left(1 - e^{\frac{-2\Delta t}{\tau}}\right) \tag{43}$$

where $\Delta\varepsilon_{f-real}^{12}$is the actual release value of $\Delta\varepsilon_f^1$ at time $t=2\Delta t$ and $\Delta\varepsilon_{f-real}^{22}$ is the actual release value of $\Delta\varepsilon_f^2$ at time $t=2\Delta t$.

Now, the actual strain is:

$$\varepsilon_{f-real}^2 = \varepsilon_f^0 + \Delta\varepsilon_f{}^1 + \Delta\varepsilon_f{}^2 - \left(\Delta\varepsilon_f^1 e^{\frac{-2\Delta t}{\tau}} + \Delta\varepsilon_f^2 e^{\frac{-\Delta t}{\tau}}\right) \tag{44}$$

At time $t=i\Delta t$ and temperature $T=T_0+i\Delta T$, the change of the frozen strain in the original model is $\Delta\varepsilon_f^i$ at the *i*th temperature increment. The changes of the frozen strains in reality are:

$$\begin{cases} \Delta\varepsilon_{f-real}^{ii} = \Delta\varepsilon_f^i\left(1 - e^{\frac{-\Delta t}{\tau}}\right) \\ \vdots \\ \Delta\varepsilon_{f-real}^{ki} = \Delta\varepsilon_f^k\left(1 - e^{\frac{-(i\Delta t-(k-1)\Delta t)}{\tau}}\right) \\ \vdots \\ \Delta\varepsilon_{f-real}^{2i} = \Delta\varepsilon_f^2\left(1 - e^{\frac{-(i-1)\Delta t}{\tau}}\right) \\ \Delta\varepsilon_{f-real}^{1i} = \Delta\varepsilon_f^1\left(1 - e^{\frac{-i\Delta t}{\tau}}\right) \end{cases} \tag{45}$$

where $\Delta\varepsilon_{f-real}^{ki}$ is the actual release value of $\Delta\varepsilon_f^k$ in time $t=i\Delta t$.

The actual strain becomes:

$$\begin{aligned} \varepsilon_{f-real}^i = {} & \varepsilon_f^0 + \Delta\varepsilon_f^1 + \Delta\varepsilon_f^2 + \cdots + \Delta\varepsilon_f^i \\ & -\left(\Delta\varepsilon_f^1 e^{\frac{-i\Delta t}{\tau}} + \Delta\varepsilon_f^2 e^{\frac{-(i-1)\Delta t}{\tau}} + \cdots + \Delta\varepsilon_f^k e^{\frac{-(i\Delta t-(k-1)\Delta t)}{\tau}}\right. \\ & \left. + \cdots + \Delta\varepsilon_f^i e^{\frac{-\Delta t}{\tau}}\right) \end{aligned} \tag{46}$$

Eq. (46) can be simplified as follows:

$$\varepsilon_{f-real}^i = \varepsilon_f^0 + \Delta\varepsilon_f^1 + \Delta\varepsilon_f^2 + \cdots + \Delta\varepsilon_f^i - \left(\sum_{k=1}^{i} \Delta\varepsilon_f^k e^{\frac{-(i\Delta t-(k-1)\Delta t)}{\tau}}\right) \tag{47}$$

In the original model, the theoretical frozen strain is $\varepsilon_f^i$ at temperature $T=T_0+i\Delta T$. It can be written as:

$$\varepsilon_f^i = \varepsilon_f^0 + \Delta\varepsilon_f^1 + \Delta\varepsilon_f^2 + \cdots + \Delta\varepsilon_f^i \tag{48}$$

Inserting Eq. (48) into Eq. (47), we have:

$$\varepsilon_{f-real}^i = \varepsilon_f^i - \left(\sum_{k=1}^{i} \Delta\varepsilon_f^k e^{\frac{-(i\Delta t-(k-1)\Delta t)}{\tau}}\right) \tag{49}$$

An integral formation of Eq. (49) is:

$$\varepsilon_{f-real} = \varepsilon_f - \int_0^t \dot{\varepsilon}_f e^{\frac{-(t-a)}{\tau}} da \tag{50}$$

#### 2.4.3. The improved constitutive equations

Furthermore, we can obtain the frozen strain in reality $\varepsilon_{f-real}$ from $\varepsilon_f$. In the calculation of the total stress, replace $\varepsilon_f$ with $\varepsilon_{f-real}$. Therefore, in the improved model, the constitutive equations of the SMPs become:

$$\begin{cases} \sigma_{total} = \frac{\varepsilon_{total}-\varepsilon_{f-real}-\varepsilon_T}{\frac{\gamma}{Eg}+\frac{1-\gamma}{Er}} \\ \frac{d\varepsilon_f}{dT} = \frac{d\gamma}{dT}[1-f(T)]\frac{\varepsilon_{total}-\varepsilon_f-\varepsilon_T}{E_r\left(\frac{\gamma}{Eg}+\frac{1-\gamma}{Er}\right)} \\ \varepsilon_{f-real} = \varepsilon_f - \int_0^t \dot{\varepsilon}_f e^{\frac{-(t-a)}{\tau}} da \end{cases} \tag{51}$$

## 3. Temperature variable function (*f*(*T*), $\gamma$) identification and material parameter determination

First, we identify the function of temperature *f*(*T*) in Eq. (11), which provides the solution of residual mechanical strain $\varepsilon_{g-mechanics}$ during the glass transition. To further explain the previous assumption and determine a reasonable function of temperature *f*(*T*), we introduce the widely accepted Flory's iso-free volume theory of the glass transition phenomena (Fox and Loshaek, 1955) into our work. In their theory, the volume of a macroscopic solid or liquid is composed of the occupied volume and free volume. The

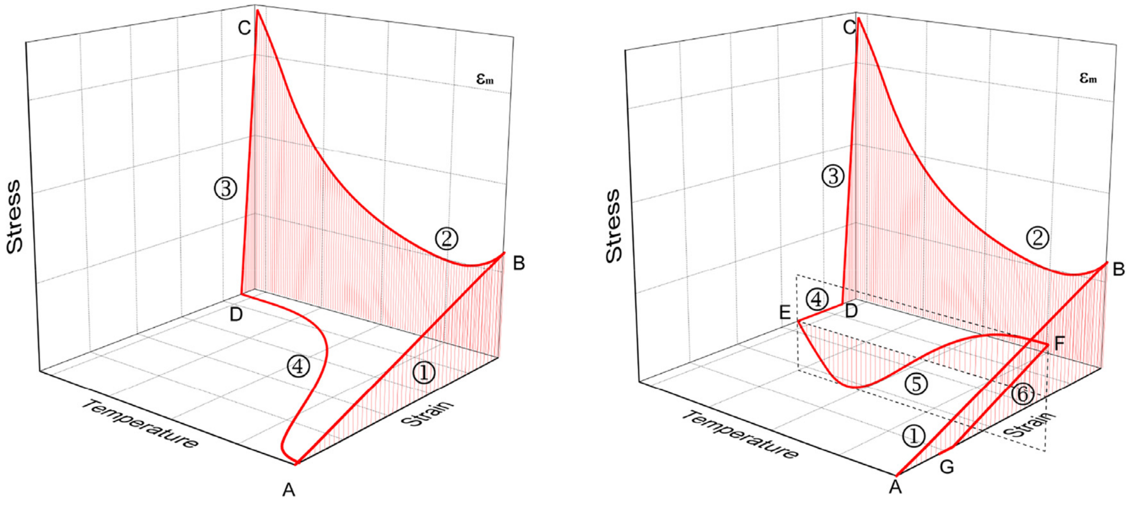

(a) (b)

**Fig. 3.** Stress-strain-temperature diagrams illustrating the SMBs of SMPs: (a) unconstrained free strain recovery case; (b) fixed strain constraints stress recovery case.

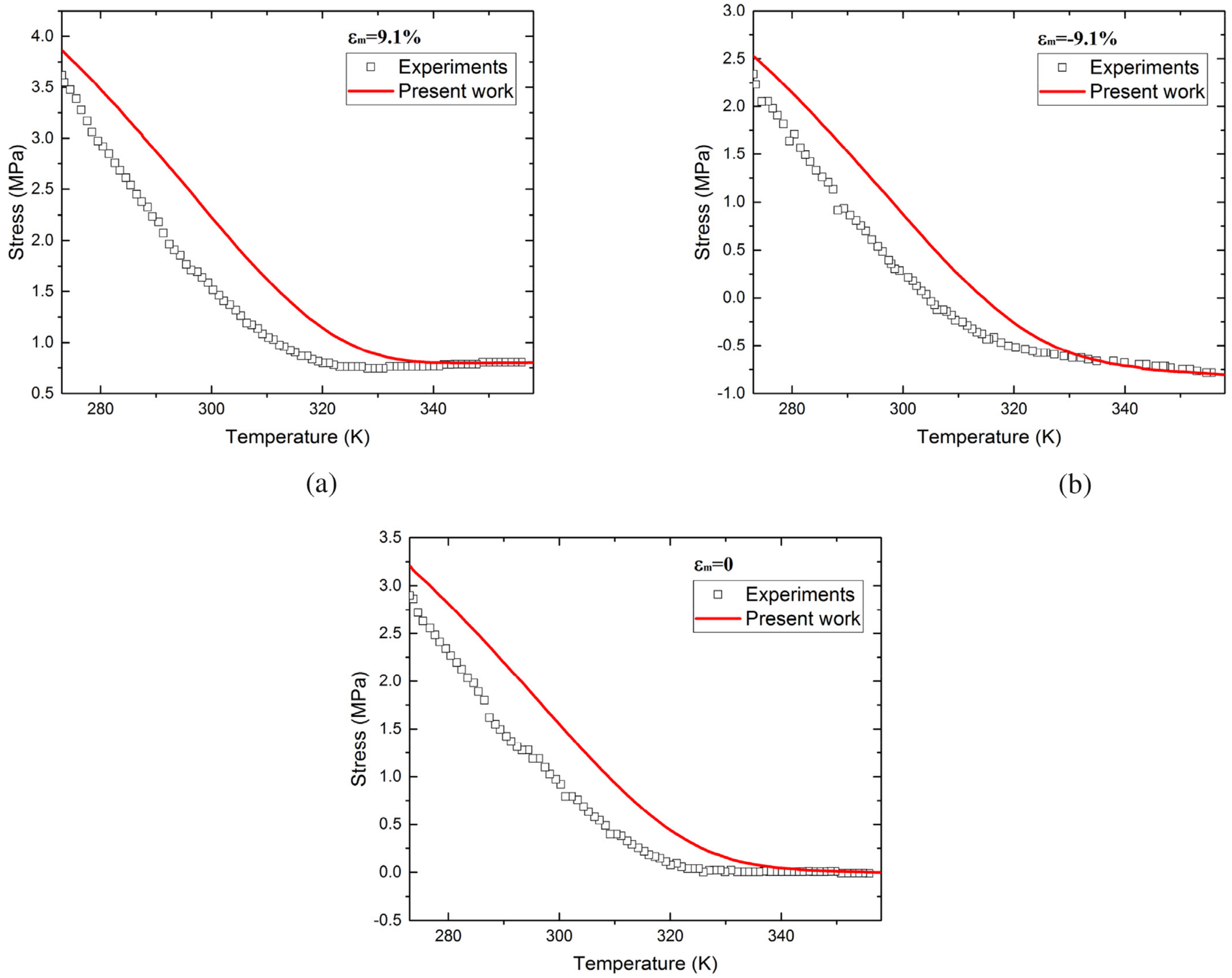

(a) (b)

(c)

**Fig. 4.** The stress–temperature results in the cooling process with different loading patterns: (a) $\varepsilon_m = 9.1\%$; (b) $\varepsilon_m = -9.1\%$; (c) $\varepsilon_m = 0$. Comparisons of the simulation results and experimental data are also shown. Experiments reported by Liu et al. (2006).

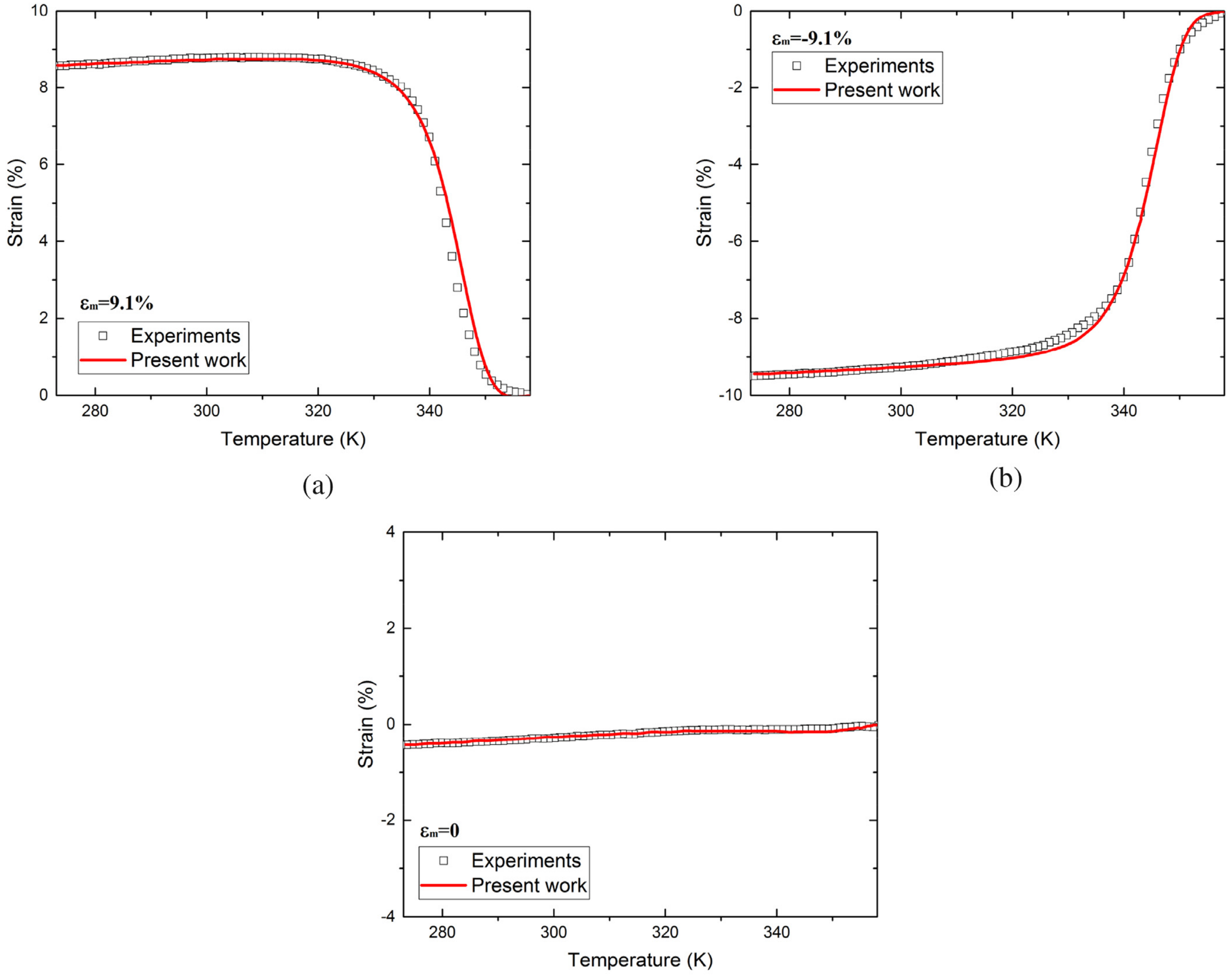

(a)

(b)

(c)

**Fig. 5.** The strain–temperature results in the cooling process with different loading patterns: (a) $\varepsilon_m = 9.1\%$; (b) $\varepsilon_m = -9.1\%$; (c) $\varepsilon_m = 0$. Comparisons of the simulation results and experimental data are also shown. Experiments reported by Liu et al. (2006).

occupied volume is the actual possession of an atomic or molecular volume and the free volume is the gap between molecules. The free volume is dispersed in the matrix with different sized holes, providing space for atomic, molecular, and molecular chain segment movement.

When the temperature is higher than the glass transition temperature $T_g$, the free volume decreases and motion of the molecular chain is restricted with the decrease in temperature. The lower the temperature, the stronger the restriction. Thus, we assume that the residual mechanical strain of glassy phase domains formed at different temperatures should be different. To simplify the problem, the residual mechanical strain in the newly formed glassy phase domains should be a linear function of the initial mechanical strain.

When the temperature is reduced to $T_g$, the free volume decreases to a minimum, and the free volume remains at the minimum value when the temperature continues to decrease. Because there is not sufficient space for chain segment movement, the chain segment motion of the newly formed glassy phase domains is completely frozen and the residual mechanical strain becomes 0.

From the analysis with iso-free volume theory above, the function of temperature $f(T)$ in Eq. (11) can be defined as:

$$f(T) = \begin{cases} \frac{T-T_g}{T_g}, & T > T_g \\ 0, & T \le T_g \end{cases} \tag{52}$$

Inserting Eq. (52) into Eq. (11), the residual mechanical strain $\varepsilon_{g-mechanics}$ during the glass transition can be obtained.

The volume fraction of the glassy phase also changes with the change in temperature. To reveal the evolutionary rules for the glassy phase volume fraction during cooling and heating, Liu et al. (2006) proposed a phenomenological function of temperature with two variables, $c$ and $n$:

$$\gamma = 1 - \frac{1}{1 + c(T_h - T)^n} = \frac{\varepsilon_f}{\varepsilon_{total}} \tag{53}$$

The volume fraction of glassy phase $\gamma$ is actually the ratio of scalar $\varepsilon_f$ to $\varepsilon_{total}$ (Liu et al., 2006). Thus, the variables $c$ and $n$ can be ascertained by fitting the experimental data $\varepsilon_f/\varepsilon_{total}$.

Using Eq. (53), we can find the volume fraction of the glassy phase $\gamma$ at different temperatures. The volume fractions of the

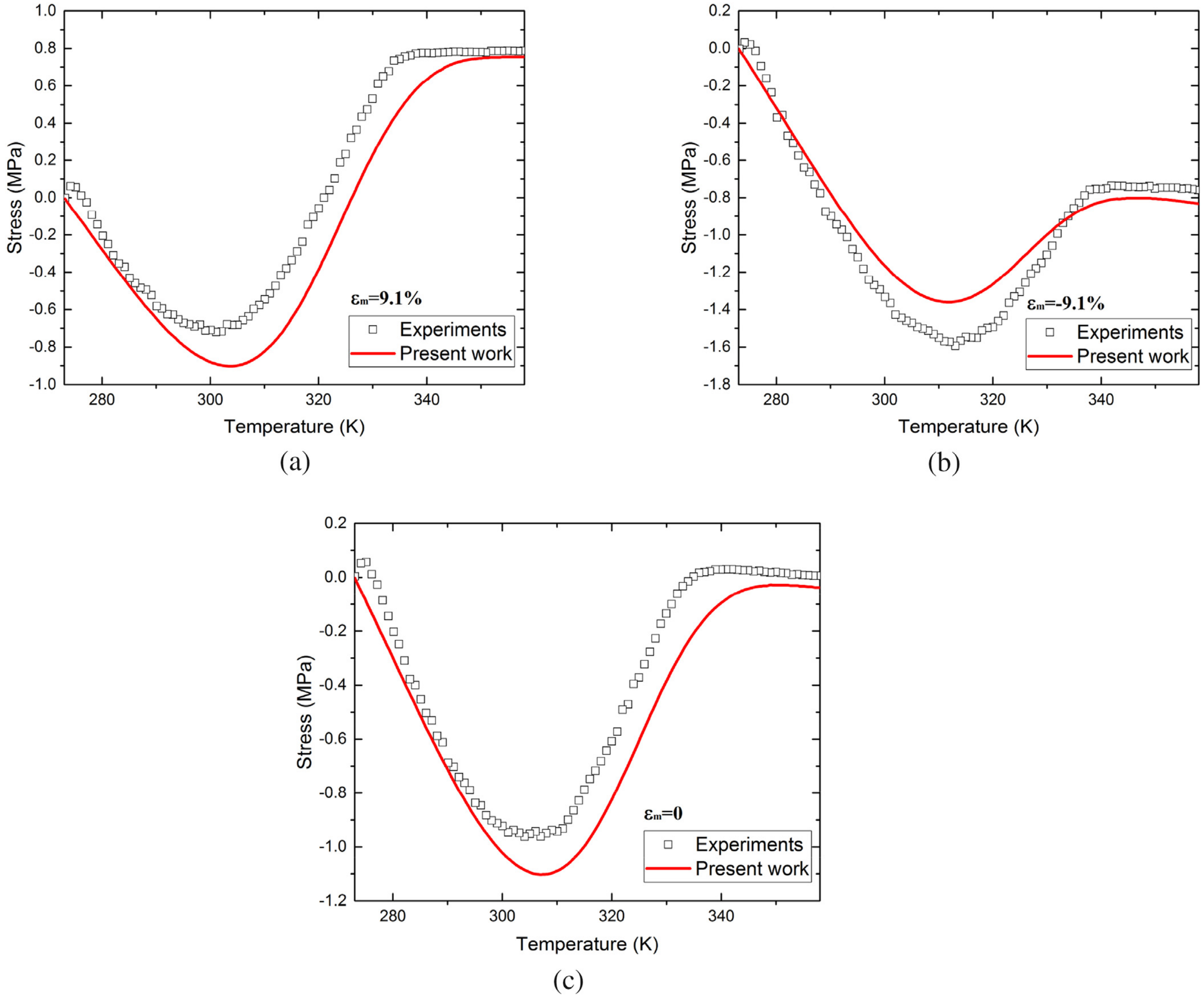

**Fig. 6.** The stress–temperature results under the strain constraint condition in the heating process with different loading patterns: (a) $\varepsilon_m = 9.1\%$; (b) $\varepsilon_m = -9.1\%$; (c) $\varepsilon_m = 0$. Comparisons of the simulation results and experimental data are also shown. Experiments reported by Liu et al. (2006).

glassy phase at temperature $T = T_h$ and $T = T_l$ are denoted by $\gamma_{T_h}$ and $\gamma_{T_l}$, respectively.

To apply this model to describe the SME of SMPs, the moduli $E_g$ and $E_r$ should be specified. The modulus of the glassy phase domains $E_g$ should be invariable in the temperature range considered (Liu et al., 2006). For the rubbery phase domains, on the other hand, $E_r$ is a defined as (Liu et al., 2006; Ward and Hadley, 1993):

$$E_r = 3NkT \tag{54}$$

where $N$ is the cross-link density of the rubbery phase polymer, $k$ is Boltzmann's constant, and $T$ is the absolute temperature.

From Eq. (51), the Young's modulus $E$ of the SMPs can be defined as:

$$E = \frac{1}{\frac{\gamma}{E_g} + \frac{1-\gamma}{E_r}} \tag{55}$$

From the isothermal uniaxial strain-stress tests at temperatures $T = T_h$ and $T = T_l$, two extreme values of the Young's modulus $E$ can be obtained, which are denoted by $E_{T_h}$ and $E_{T_l}$, respectively. At temperature $T = T_h$, $\gamma = \gamma_{T_h}$, $E = E_{T_h}$ and at temperatures $T = T_l$, $\gamma = \gamma_{T_l}$, $E = E_{T_l}$, two equations based on Eq. (55) can be formulated. Solving these two equations together, the modulus $E_g$ and cross-link density $N$ can be obtained.

## 4. Model verification

Thus far, the required material parameters in the continuum thermomechanical constitutive model can be fully determined with the relevant experimental data. In this section, we verify the validity of the proposed continuum thermomechanical constitutive model by comparing the numerical simulation results of SMBs with the experimental observations available in the literature. To show the broad applicability of our model, we will reproduce the SMBs of two different materials: that from the experiments on an epoxy resin SMP performed by Liu et al. (2006) and that from the experiments on an acrylate network composition SMP performed by Arrieta et al. (2014a, b).

In the above mentioned experiments, the thermomechanical cycles of two types of SMPs are investigated: the free strain recovery process and fixed strain constraint stress recovery process. A general 3D stress-strain-temperature diagram of the SMPs in the unconstrained free strain recovery case is illustrated in Fig. 3(a). Typically, the SMB cycles can be divided into four processes. In

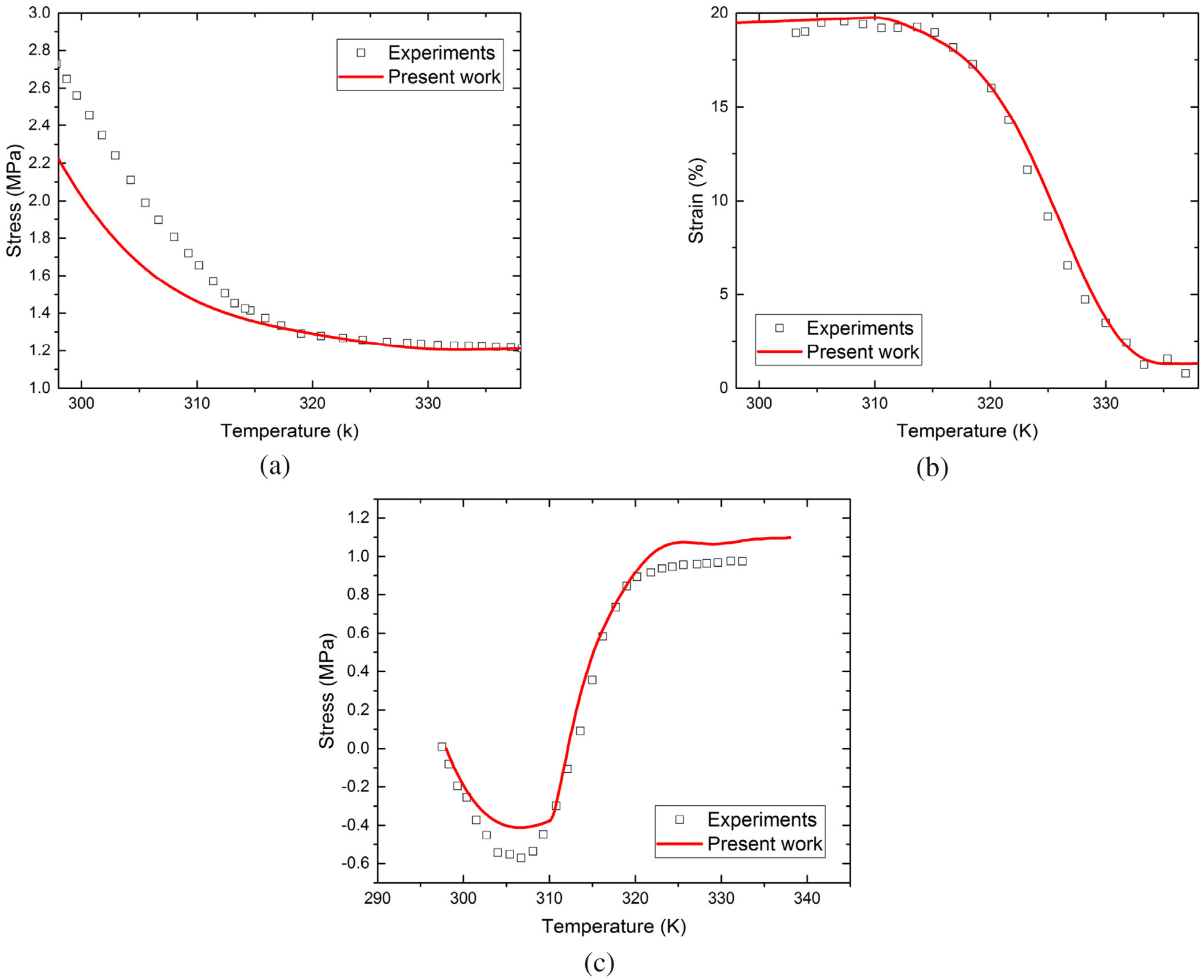

**Fig. 7.** Reproduction of the SME by the continuum thermomechanical constitutive model: (a) stress–temperature results under the free strain condition in the cooling process; (b) strain–temperature results under the free strain condition in the heating process; (c) stress–temperature results under the strain constraint condition in the heating process. Comparisons of the simulation results and experimental data are also shown. Experiments reported by Arrieta et al. (2014a, b).

the first process (loading), a mechanical load is applied to SMPs at an elevated temperature $T_h$. The specimen is pre-deformed from the original state “A” (non-stress and non-strain) to a state of pre-deformation “B”. In the second process (cooling), the specimen is cooled to a lower temperature $T_l$ (state “C”) with the pre-strain $\varepsilon_m$ maintained. Followed by the third process (unloading), the strain constraint conditions are removed from the specimen at temperature $T_l$ (from state “C” to state “D”). In the last process, the SMP specimen is reheated to a high temperature $T_h$ under the free strain condition. To explore the stress and strain responses of SMPs under flexible external constraints, the fixed strain constraint stress recovery case is often investigated. The general 3D stress-strain-temperature diagram is illustrated in Fig. 3(b). The entire case can be divided into six processes. The initial processes ①→②→③ are the same as those in the unconstrained free strain recovery case. In the fourth process, the unloading condition is kept at temperature $T_l$ for some time. In the fifth process, the SMP specimen is reheated to the high temperature $T_h$ under a fixed strain constraint. In the last process, the specimen is unloaded at temperature $T_h$.

**Table 1**
Material parameters adopted from the experiments reported by Liu et al. (2006).

| Material parameters | Units | Values |
|---|---|---|
| $T_g$ | $[K]$ | 343 |
| $T_h$ | $[K]$ | 358 |
| $T_l$ | $[K]$ | 273 |
| $n$ | [-] | 4 |
| $c$ | $[1/K^4]$ | $2.76 \times 10^{-5}$ |
| $E_g$ | $[MPa]$ | 813 |
| $N$ | $[mol/m^3]$ | 986 |
| $\alpha$ | $[K^{-1}]$ | $-3.16 \times 10^{-4} + 1.42 \times 10^{-6} T$ |
| $\tau$ | $[s]$ | 1 |

### 4.1. Model validation using epoxy resin experimental data

To test the stability of the model, we reproduce the SME of an epoxy resin under different loading patterns (tension, zero-strain and compression). We simulate the experimental process reported by Liu et al. (2006), and the model parameters used are shown in Table 1. All of the model parameters are determined by the parameter identification procedure described in Section 3.

**Table 2**
Material parameters adopted from the experiments reported by Arrieta et al. (2014a, b).

| Material parameters | Units | Values |
|---|---|---|
| $T_g$ | $[K]$ | 310 |
| $T_h$ | $[K]$ | 338 |
| $T_l$ | $[K]$ | 298 |
| $n$ | [-] | 4 |
| $c$ | $[1/K^4]$ | $3.6001 \times 10^{-5}$ |
| $E_g$ | $[MPa]$ | 8538.93 |
| $N$ | $[mol/m^3]$ | 719.28 |
| $\alpha$ | $[K^{-1}]$ | $-2.066 \times 10^{-4} + 1.52 \times 10^{-6}T$ |
| $\tau$ | $[s]$ | 10,000 (at $T \leq T$) 10 (at $T > T_{g)}$ |

For the unconstrained free strain recovery case, the stress-temperature results in a cooling process and strain-temperature results in a heating process with different pre-strains, as shown in Figs. 4 and 5. The simulated results are in good agreement with the experimental results, indicating that the model has the ability to describe the SMPs' stress response in the cooling process and predict the strain variation in the reheating process with different loading patterns.

For the fixed strain constraint stress recovery case, the stress-temperature results during the heating process are shown in Fig. 6. From Fig. 6, it can be seen that the modeling results agree well with the experimental data. Therefore, this model can also be used to predict the stress and strain responses of SMPs under flexible external constraints.

### *4.2. Model validation using acrylate polymer network experimental data*

To show the broad applicability of the model, we use the proposed model to describe the SMB of another material, an acrylate polymer network. We simulate the experiments reported by Arrieta et al. (2014a, b), and the material parameters used are presented in Table 2. The reproduction of the SME by the continuum thermomechanical constitutive model is shown in Fig. 7. Fig. 7(a) and (b) show the stress–temperature results in the cooling process and strain–temperature results in the heating process in the free strain recovery case. From Fig. 7(a) and (b), it can be seen that the model is able to reproduce the SME of this material in the free strain recovery cycle process quite well. For a fixed strain constraint stress recovery case (as shown in Fig. 7(c)), a remarkable consistency between the simulation results and experiments can also be obtained. Under flexible external constraints, the stress variation with temperature is quite complex. The proposed model can precisely reproduce the stress slumps phenomenon in the initial phase of the heating process, increasing around $T_g$ and almost remaining constant in the vicinity of $T_h$. This cannot be observed in the results if we don't consider the time factor in the model.

## 5. Concluding remarks

In this paper, a thermomechanical constitutive model based on glass transition and the concept of frozen strain release rate is proposed to predict the shape memory behaviors of amorphous SMPs. The proposed model considers the materials as a mixture of a rubbery phase and glassy phase and thus it can physically describe the glass transition in SME. In addition, the model is further improved by introducing a time factor to make it more feasible. To test its validity and applicability, the model is adopted to predict the SME of two differently shaped memory materials under free strain and strain constraint conditions. The comparisons of the simulated results and experimental observations are remarkably consistent, indicating that our model can be used for various SMPs. This model can be used not only to predict the strain or stress response of SMPs under the free strain condition but also to reproduce the SMB under various flexible external constraints. We hope that the proposed approach will be a valuable tool for future theoretical and experimental research on SMPs. Although we introduced the time factor into the model, the viscosity of polymers is still not considered in the present work. This factor should be considered in future works.

## Acknowledgment

The authors are grateful for support from the National Natural Science Foundation of China through grant numbers 11372236 and 11572236.

## References

Arrieta, J.S., Diani, J., Gilormini, P., 2014a. Cyclic and monotonic testing of free and constrained recovery properties of a chemically crosslinked acrylate. J. Appl. Polym. Sci. 131.

Arrieta, S., Diani, J., Gilormini, P., 2014b. Experimental characterization and thermo-viscoelastic modeling of strain and stress recoveries of an amorphous polymer network. Mech. Mater. 68, 95–103.

Ashrafi, M.J., Arghavani, J., Naghdabadi, R., Sohrabpour, S., Auricchio, F., 2016. Theoretical and numerical modeling of dense and porous shape memory alloys accounting for coupling effects of plasticity and transformation. Int. J. Solids Struct. 88–89, 248–262.

Baghani, M., Naghdabadi, R., Arghavani, J., Sohrabpour, S., 2012. A thermodynamically-consistent 3D constitutive model for shape memory polymers. Int. J. Plast. 35, 13–30.

Barot, G., Rao, I., 2006. Constitutive modeling of the mechanics associated with crystallizable shape memory polymers. Zeitschrift für angewandte Mathematik und Physik ZAMP 57, 652–681.

Behl, M., Razzaq, M.Y., Lendlein, A., 2010. Multifunctional shape-memory polymers. Adv. Mater. 22, 3388–3410.

Chen, Y.-C., Lagoudas, D.C., 2008a. A constitutive theory for shape memory polymers. Part I. J. Mech. Phys. Solids 56, 1752–1765.

Chen, Y.-C., Lagoudas, D.C., 2008b. A constitutive theory for shape memory polymers. Part II. J. Mech. Phys. Solids 56, 1766–1778.

Diani, J., Gilormini, P., Frédy, C., Rousseau, I., 2012. Predicting thermal shape memory of crosslinked polymer networks from linear viscoelasticity. Int. J. Solids Struct. 49, 793–799.

Fox, T., Loshaek, S., 1955. Influence of molecular weight and degree of crosslinking on the specific volume and glass temperature of polymers. J Polym. Sci. Part A Polymer Chemistry 15, 371–390.

Ge, Q., Luo, X., Iversen, C.B., Nejad, H.B., Mather, P.T., Dunn, M.L., Qi, H.J., 2014. A finite deformation thermomechanical constitutive model for triple shape polymeric composites based on dual thermal transitions. Int. J. Solids Struct. 51, 2777–2790.

Ge, Q., Luo, X., Rodriguez, E.D., Zhang, X., Mather, P.T., Dunn, M.L., Qi, H.J., 2012. Thermomechanical behavior of shape memory elastomeric composites. J. Mech. Phys. Solids 60, 67–83.

Ge, Q., Serjouei, A., Qi, H.J., Dunn, M.L., 2016. Thermomechanics of printed anisotropic shape memory elastomeric composites. Int. J. Solids Struct. 102–103, 186–199.

Ge, Q., Westbrook, K.K., Mather, P.T., Dunn, M.L., Qi, H.J., 2013. Thermomechanical behavior of a two-way shape memory composite actuator. Smart Mater. Struct. 22, 955–962.

Ghosh, P., Reddy, J.N., Srinivasa, A.R., 2013. Development and implementation of a beam theory model for shape memory polymers. Int. J. Solids Struct. 50, 595–608.

He, Y., Guo, S., Liu, Z., Liew, K.M., 2015. Pattern transformation of thermo-responsive shape memory polymer periodic cellular structures. Int. J. Solids Struct. 71, 194–205.

Hu, J., Zhu, Y., Huang, H., Lu, J., 2012. Recent advances in shape–memory polymers: structure, mechanism, functionality, modeling and applications. Prog. Polym. Sci. 37, 1720–1763.

Hu, J.L., Chen, S.J., 2010. A review of actively moving polymers in textile applications. J. Mater. Chem. 20, 3346–3355.

Huang, W.M., Song, C.L., Fu, Y.Q., Wang, C.C., Zhao, Y., Purnawali, H., Lu, H.B., Tang, C., Ding, Z., Zhang, J.L., 2013. Shaping tissue with shape memory materials. Adv. Drug Deliv. Rev. 65, 515–535.

Ju, H.K., Kang, T.J., Yu, W.R., 2010. Thermo-mechanical constitutive modeling of shape memory polyurethanes using a phenomenological approach. Int. J. Plast. 26, 204–218.

Leng, J., Lu, H., Liu, Y., Huang, W.M., Du, S., 2009. Shape-memory polymers—a class of novel smart materials. MRS Bull. 34, 848–855.

Li, Y., Guo, S.-S., He, Y., Liu, Z., 2015. A simplified constitutive model for predicting shape memory polymers deformation behavior. Int. J. Comput. Mater. Sci. Eng. 04, 1550001.

Li, Y., He, Y., Liu, Z., 2017. A viscoelastic constitutive model for shape memory polymers based on multiplicative decompositions of the deformation gradient. Int. J. Plast. 91, 300–317.

Lin, J., Chen, L., 1999. Shape-memorized crosslinked ester-type polyurethane and its mechanical viscoelastic model. J. Appl. Polym. Sci. 73, 1305–1319.

Liu, Y., Gall, K., Dunn, M.L., Greenberg, A.R., Diani, J., 2006. Thermomechanics of shape memory polymers: uniaxial experiments and constitutive modeling. Int. J. Plast. 22, 279–313.

Liu, Z., Toh, W., Ng, T.Y., 2015. Advances in mechanics of soft materials: a review of large deformation behavior of hydrogels. Int. J. Appl. Mech. 735.

Matsumura, T., Nakamura, T., Tetsuka, M., Takashina, K., Nishi, K.T.Y., 2011. Shape Memory Ceramics, 604 Mrs Online Proceeding Library.

Matsuoka, S., 1992. Relaxation Phenomena in Polymers. Hanser Munich etc..

Morshedian, J., Khonakdar, H.A., Rasouli, S., 2005. Modeling of shape memory induction and recovery in heat-shrinkable polymers. Macromol. Theory Simul. 14, 428–434.

Oliveira, S.A., Savi, M.A., Santos, I.F., 2014. Uncertainty analysis of a one-dimensional constitutive model for shape memory alloy thermomechanical description. Int. J. Appl. Mech. 6, 1450067.

Poorasadion, S., Arghavani, J., Naghdabadi, R., Sohrabpour, S., 2015. Implementation of microplane model into three-dimensional beam element for shape memory alloys. Int. J. Appl. Mech. 7, 1550091.

Qi, H.J., Nguyen, T.D., Castro, F., Yakacki, C.M., Shandas, R., 2008. Finite deformation thermo-mechanical behavior of thermally induced shape memory polymers. J. Mech. Phys. Solids 56, 1730–1751.

Rajagopal, K., Srinivasa, A., 1998a. Mechanics of the inelastic behavior of materials—Part 1, theoretical underpinnings. Int. J. Plast. 14, 945–967.

Rajagopal, K., Srinivasa, A., 1998b. Mechanics of the inelastic behavior of materials. Part II: inelastic response. Int. J. Plast. 14, 969–995.

Rossiter, J., Takashima, K., Scarpa, F., Walters, P., Mukai, T., 2014. Shape memory polymer hexachiral auxetic structures with tunable stiffness. Smart Mater. Struct. 23, 11.

Strobl, G.R., 1997. Metastable partially crystalline states, The Physics of Polymers. Springer, pp. 143–190.

Tobushi, H., Hashimoto, T., Hayashi, S., Yamada, E., 1997. Thermomechanical constitutive modeling in shape memory polymer of polyurethane series. J. Intell. Mater. Syst. Struct. 8, 711–718.

Tobushi, H., Okumura, K., Hayashi, S., Ito, N., 2001. Thermomechanical constitutive model of shape memory polymer. Mech. Mater. 33, 545–554.

Ward, I.M., Hadley, D.W., 1993. An Introduction to the Mechanical Properties of Solid Polymers. John Wiley & Sons Ltd.; John Wiley & Sons, Inc.

Westbrook, K.K., Parakh, V., Chung, T., Mather, P.T., Wan, L.C., Dunn, M.L., Qi, H.J., 2010. Constitutive modeling of shape memory effects in semicrystalline polymers with stretch induced crystallization. J. Eng. Mater. Technol. 132, 427–438.

Xie, T., 2010. Tunable polymer multi-shape memory effect. Nature 464, 267–270.

Xu, We, Li, Guoqiang, 2010. Constitutive modeling of shape memory polymer based self-healing syntactic foam. Int. J. Solids Struct. 47, 1306–1316.

Yang, Q., Li, G., 2016. Temperature and rate dependent thermomechanical modeling of shape memory polymers with physics based phase evolution law. Int. J. Plast. 80, 168–186.